CORA Cork Open Research Archive
Cartlann Taighde Oscailte Chorcaí

Title	Bottom-up growth of fully transparent contact layers of indium tin oxide nanowires for light-emitting devices
Authors	O'Dwyer, Colm;Szachowicz, Marta;Visimberga, Giuseppe;Lavayen, Vladimir;Newcomb, Simon B.;Sotomayor Torres, Clivia M.
Publication date	2009-02-01
Original Citation	O'Dwyer, C., Szachowicz, M., Visimberga, G., Lavayen, V., Newcomb, S. B. and Sotomayor Torres, C. M. (2009) 'Bottom-up growth of fully transparent contact layers of indium tin oxide nanowires for light-emitting devices', Nature Nanotechnology, 4, pp. 239-244. http://dx.doi.org/10.1038/nnano.2008.418
Type of publication	Article (peer-reviewed)
Link to publisher's version	10.1038/nnano.2008.418
Rights	© 2009 Macmillan Publishers Limited. All rights reserved.
Download date	2024-04-20 04:23:38
Item downloaded from	https://hdl.handle.net/10468/2821

UCC
University College Cork, Ireland
Coláiste na hOllscoile Corcaigh

Bottom-up growth of fully transparent contact layers of indium tin oxide nanowires for LEDs

C. O'Dwyer,[a,*] M. Szachowicz,[b] G. Visimberga,[b] V. Lavayen,[c,†] S. B. Newcomb,[d] C. M. Sotomayor Torres[e,f]

[a] *Department of Physics, and Materials & Surface Science Institute, University of Limerick, Limerick, Ireland*

[b] *Tyndall National Institute, University College Cork, Cork, Ireland*

[c] *Departamento de Física, Universidad Técnica Federico Santa María, Valparaíso 2390123, Chile*

[d] *Glebe Scientific Limited, Newport, Co. Tipperary, Ireland*

[e] *Institute for Research and Advanced Studies, ICREA, 08010 Barcelona, Spain*

[f] *Catalan Institute of Nanotechnology, Edifici CM7, Campus Universitat Autonoma de Barcelona, 08193 Bellaterra (Barcelona), Spain*

**Email: colm.odwyer@ul.ie; Tel: +353 61 202288; Fax: +353 61 213529*

Thin layers of indium tin oxide (ITO) are widely used as transparent coatings and electrodes in solar energy cells [1], flat-panel displays [2,3], anti-reflection coatings [4] and radiation protection [5] because they display low resistivity, strong absorption at ultraviolet wavelengths, high transmission in the visible [6], high reflectivity in the far-infrared and strong attenuation in the microwave region. However, there is often a trade-off between electrical conductivity and transparency at visible wavelengths for ITO and other transparent conducting oxides. Here we report the growth of layers of ITO nanowires that exhibit optimum electronic and photonic properties and demonstrate their use as fully transparent top contacts in the visible to near-infrared region for light emitting devices (LEDs).

As the most important transparent conducting oxide, tin-doped indium oxide has also found a wide range of applications from photovoltaics to Li-ion battery materials [7]. The fabrication techniques of homogeneous 1-D nanostructures have pursued the control over shape, aspect ratio, and crystalline arrangement to a considerable degree [8-10], and the improvement of the synthesis methods [11-13] has recently achieved the direct integration of functional nanostructures into nanodevices [14-16].

One particular application of ITO that employs its conductive and transmissive properties, is that of an ohmic contact for LEDs, but has until now, only had limited success due to high resistivities and an unacceptable trade-off between its electrical and optical characteristics. The limited availability of materials with desired refractive indices, however, has prevented the implementation of optical components with very high performance. The possibility of forming controlled complex, multi-level branched structures [17] with optimized optical properties in a single-step, bottom-up growth regime, is a real advance considering their compatibility with optoelectronic device architectures.

We have developed a simple, reproducible and controllable molecular beam epitaxial growth system for obtaining high quality, uniphasic, branched ITO nanowires on silicon and oxidised silicon surfaces using In and Sn precursors in an oxygen atmosphere. The nanowire layer morphology and transparency can be tailored through rational control of the evaporation-condensation parameters, and will be shown to result in bottom-up grown layers of self-catalysed and seeded nanowires with excellent electrical, optical and homogeneous structural properties, that can even be grown as large area (several cm^2) contacts. They will also be shown to be an improved replacement option for the standard NiCr top contact on a Si/SiGe multi-quantum well (MQW) LED, exhibiting a transparency of >80% in the visible and >90% in the 1.2-1.6 μm range.

The main structural features of the nanowire layer growth are shown in Fig. 1. The entire process occurs in one step: seeding, nucleation, growth, and progressive branch seeding and growth. The initial stage involves the seeding of the substrate; here, oxidised In-Sn droplets condense on the substrate surface, as shown in Fig. 1a, which form the nucleation seeds for subsequent nanowire growth; other large area

examples of the substrate seeding can be found in the Supporting Information, Fig. S1. Figure 1b shows an SEM image of a region of a fully grown nanowire layer. Further representative images of the nanowire layer morphology are found in the Supporting Information, Fig. S2. Each nanowire (backbone and branches) is terminated with a uniphasic seed crystal, a typical example of which is shown in Fig. 1c. Crystallographic precipitation leads to non-tapered homogeneous nanowire growth. HRTEM analysis of the nanowires in Fig. 1d shows a cubic structure; SEM observations show a square cross-section for all nanowires confirmed by the HRTEM data evidencing nanowire growth along [100]. HRSEM and focused ion beam (FIB) milling of the seed-wire interface to remove the seed crystal (shown in Supporting Information, Fig. S2) shows the expected square cross-section due growth from the [100] faces of the cubic structure seed, further confirmed by the HRTEM of the nanowire in Fig. 1d where we observe equally spaced (002) and (020) interplanar distances of 0.506 nm, and also by X-ray diffraction (XRD) (Supporting Information, Fig. S1) where the phase is identified to be cubic $(In_{1.875}Sn_{0.125})O_3$ for which a_0 is 1.0124 nm. At initial stages of growth, these nanowires typically have diameters of 8-20 nm and lengths of 40-500 nm. The EDX spectra of the nanowires in Fig. 1e confirm that individual wires comprise In, Sn and O equivalent to 5.9 atom% of Sn inclusion in In_2O_3 (6.25% is the theoretical maximum for $(In_{1.875}Sn_{0.125})O_3$).

An overview of the typical morphological variations as a function of growth rate and substrate temperature is shown in Supporting Information, Fig. S3. We report a distinct growth mode modification from compact (but rough and partially porous) layers to dendritic nanowire growth during deposition. Locally increased porosity is the main defect found in graded index porous layer growth by oblique angle deposition techniques; such problems are not encountered for dense, highly branched nanowire layers. No heterogeneous catalysts are required and we still observe extremely high quality, defect-free nanowires comprising the layers. At very low deposition rates, porous ITO layers are found (refer to Supporting Information, Fig. S4), while at higher deposition rates single-crystal nanowires are formed.

After the growth was optimized on both quartz and silicon substrates, the growth method was applied to corresponding n-i-p^+ Si/SiGe MQW device structures, specific details of which can be found in the Supporting Information, Fig. S5. An example of an ITO nanowire layer grown on the Si/SiGe MQW structure is shown in the SEM image in Fig. 2a with a corresponding device schematic shown in Fig. 2b. Figure 2c shows the electrical characteristics of the ITO nanowire top-contacted Si/SiGe MQW LEDs measured at room temperature. The LEDs with the nanowire contact layer exhibit a forward-bias turn-on voltage of 0.55 V at an injection current of 10 mA, which is a marked improvement over LEDs and quantum cascade lasers (QCLs) with oxidized Ni/Au, Ni/Cr or thin film ITO/Ag/ITO sandwich contacts [3]. We conducted electrical measurements on a series of nanowire-containing segments using corner contacts to areas of the nanowire layer in the van der Pauw geometry [18]. The conductivity of the pure $(In_{1.875}Sn_{0.125})O_3$ branched nanowires is typically measured to be 1053.5 ± 42.3 S cm^{-1} at room temperature, which is similar to the values previously reported for other individual nanowires and two orders of magnitude greater than individual In_2O_3 or SnO_2 nanowires [2]. We note that our conductivity values are similar to those reported previously [16] for Sn-doped (5-8 atom%) In_2O_3 nanowires, whereas that of In_2O_3 nanowires without intentional doping is of the order of 1 S cm^{-1}.

The inset to Fig. 2c shows the current-voltage (I-V) characteristics of nanowire ITO contacts to the p^+-Si capping layer on the SiGe MQW at room temperature (295 K). The as-deposited nanowire layer exhibits a linear electrical behaviour even without the need for prior annealing or a metallic interlayer to curb high contact resistances, indicating a good ohmic contact. An advantage of the nanowire morphology chosen in this case is that the spherical seed prevents unwanted field emission known to occur for sharp-tipped ITO nanowires [19]. Thus, by choosing a medium temperature of 575^{o}C, we can optimize the values for sheet resistance to over four orders of magnitude lower than currently available for known transparent conducting oxides.

Nanowire layer capacitance measurements were conducted using a capacitance bridge technique [20] to determine the field effect mobilities and free carrier densities. The mobilities and the free carrier

densities are shown in Fig. 2d as a function of oxygen pressure. Oxidative crystallization of the ITO with increasing oxygen pressure contributes to the increased mobilities and carrier densities. The mobilities of the present nanowire layers are typically 55-65 $cm^2\ V^{-1}\ s^{-1}$ for oxygen pressures in the range 2-4 $\times 10^{-4}$ mbar and are comparable to In_2O_3 nanowires on oxide dielectrics (μ = 7-280 $cm^2\ V^{-1}\ s^{-1}$) and bulk monocrystalline In_2O_3 (μ = 160 $cm^2\ V^{-1}\ s^{-1}$) [21].

As mentioned above, the growth rate and temperature are key parameters in the eventual morphology of the ITO nanowire layers. To assess this influence on the optical transmission, ITO layers of varied thickness and morphology were grown on quartz substrates. Figure 3a shows their transmission spectra in the wavelength range 400-1600 nm. The inset shows a typical ITO nanowire layer deposited on a glass cover slip. The transparency in the visible range improves to ~90% with increasing growth rate up to 0.2 nm s^{-1}. Spectroscopic ellipsometric measurements show effective refractive indices of the nanowire layer-air interface to be between 1.04-1.12 for all samples investigated, directly due to the varied porosity of the nanostructured layers, calculated using the Bruggemann effective medium approximation. This is very advantageous as previous efforts to couple high transmission and low resistivity resorted to ITO/Ag/ITO multilayer sandwiches to combine the improved conductivity of Ag and the high refractive index of the ITO (η = 2.19) to boost transmittance of the metal interlayer [6,22]. The measured absorption edge for the nanostructured ITO films is ~380 nm, a value lower than that for ITO on glass and comparable to ITO/YSZ lattice matched thin films and nanowires [19].

In terms of evaluating the improvement afforded by such nanowire layers as advanced electro-optical device top contacts, the calculated reflectivity at near-normal incidence (10^o) as a function of wavelength was determined and is shown in Fig. 3b for the ITO nanowire layer, a porous ITO layer (cf. Fig. S4, Supporting Information), a thin ITO film and a standard antireflection layer of ITO on glass. ITO nanowire layers on silicon exhibited much lower reflectivity than either dense ITO on silicon or porous ITO layers in the wavelength region of interest. Only antireflection ITO coatings on glass showed similar transmission between 850-975 nm, but with an unacceptable sheet resistivity of ~15 Ω cm. Fresnel

reflection associated with higher refractive index ITO thin films is virtually eliminated [23] due to reduction in the refractive index from the substrate to the nanowire layer/ambient interface, where the refractive index was measured to vary from 2.19 (close to the substrate) to 1.04 (at the air interface). The low refractive index nanowire layer is optically specular and exhibits a 'dark' surface (see Fig. 3a), confirming the absence of Fresnel reflection over a broad spectral width. This is particularly important for LED applications because of the isotropic emission from the active region and the fact that reflection phenomena can limit the light-extraction efficiency.

Typically, ITO and other transparent conducting oxides fail to transmit light in the near infrared region above ~1.1 μm, thus preventing their employment as electrodes for LEDs operating in the second (1.3μm) and third (1.55μm) optical communications energy windows. This is due to the onset of a metal-like behaviour at low photon energies, where quanta of incident electromagnetic radiation can couple to plasma oscillations. The surface plasmon resonance (SPR) of ITO (determined using the Drude free-electron model and three-phase Fresnel equations of reflection) is observed at a much lower energy than for metals (where it generally falls into the visible range) [6]. In Fig. 3b, the surface plasmon resonance of the ITO nanowire layer (6895 cm^{-1}) compared to a thin ITO film (10204 cm^{-1}) is red-shifted by ~480 nm, pushing the onset of reflectance further towards the near to mid-IR. The minimum in reflectivity is routinely observed in the crucial 1.2-1.6 μm range at near-normal incidence (0-10^{o}). Angle-resolved reflectance measurements (Supporting Information, Fig. S6) conclusively show that the position of the surface plasmon resonance blue-shifts with increasing angle; the window for maximum transmission over the widest wavelength range is observed near-normal to the surface. Their suitability to silicon-based LEDs, is demonstrated by investigation of the room temperature electroluminescence (EL) emission from the nanowire contacted SiGe MQW LED, shown in Fig. 3c, showing unambiguously that the Si and SiGe emission lines are fully resolved through the nanowire layer contact in ambient laboratory conditions.

The low-temperature photoluminescence spectrum of the uncoated structure is shown in Fig. 4a. We observe the standard SiGe no-phonon- ($SiGe^{NP}$) and the SiGe transverse optical phonon-assisted ($SiGe^{TO}$) emission lines separated by ~56 meV [24]. The lower curve in Fig. 4a was recorded from the structure contacted with 30 nm NiCr. We observe the photoluminescence signal of the NiCr coated structure to be relatively weak, particularly for crucial excitonic recombinatorial routes. The photoluminescence intensity is attenuated in this case by ~97%, necessitating the use of a similar contact with high transmission in the wavelength range of use.

The corresponding comparative spectra of both the uncoated MQW and nanostructured ITO-contacted MQW are shown in Fig. 4b, where a marked improvement in transmission compared to the NiCr contacted MQW is observed. The highest attenuation was noted for the Si^{EHD} emission, although 20% of the uncoated MQW signal for this line was still transmitted, as opposed to negligible transmission through the NiCr contact. The $Si_{BE}{}^{TO}$ emission was attenuated by ~50% but of utmost interest are the SiGe emission lines, which were transmitted with negligible absorption. It is clear that the full spectrum (all important transitions) of a SiGe MQW LED can be resolved through the ITO nanowire top contact. Electroluminescence measurements as a function of temperature were also acquired from the ITO-contacted SiGe MQWs and are reproduced in Fig. 4c. The data indicate an excellent temperature stability in the optoelectronic properties of the nanowire layer as a top contact. The SiGe band-edge electro- and photoluminescence can be detected up to room temperature and no saturation was observed even with injection current densities greater than 1125 mA cm^{-2} (electroluminescence) and at excitation power densities >2500 W cm^{-2} (photoluminescence) (see Supporting Information, Fig. S7), indicating a very high diode quality with no electro-optical deterioration in the nanowire contacts.

Light, in this case the SiGe emission lines, escapes the nanowire layer due to its unusually low effective refractive index [25]. The escape cone for light in bulk ITO of refractive index $\eta = 2.19$, covers an effective solid angle (Ω) of 0.65 sr, given by $\Omega = 2\pi \cdot (1 - \cos\omega)$ sr. The key to increasing the light escape probability is to allow multiple opportunities for photons to find the escape cone, emit and be

detected. For the ITO nanowire layer with a refractive index of 1.04 for the nanowire layer-air interface, the solid angle for the escape cone increases to ~2.9 sr. This allows an efficient mechanism that redirects photons that were originally emitted out of the escape cone, back into the escape cone to boost external efficiency. The geometry of the nanowire layer maximizes transmission through a single-step, practical approach of randomizing scattering photons. In addition, the emission is maximised by the angular dependence of the plasma frequency, where the transmission is both maximized and limited to near-normal output. The optical and electrical properties as a whole are unprecedented for any conductive, transparent oxide and have the added benefit of being experimentally much simpler than more complex, multi-step deposition of several defect-free layers of reducing refractive index (exhibiting poor conductivities) and highly conducting thin films (exhibiting poor transmission in the visible region).

Thus, the ability of fabricating high axial-ratio monocrystalline and highly transparent doped metal-oxide nanowire layers with unprecedented simplicity in morphological control and phase homogeneity proves to be an excellent transparent top contact to LEDs. The effective rational control of the entire novel, one-step growth process affords controllable large area nanowire layer fabrication without external catalysts under device growth conditions, exhibiting optimum electrical and optical characteristics. Modifications and extensions of the technique can be envisaged for similar materials, such as IZO and related compounds, and possibly for tunable antireflection coatings.

Acknowledgments

The support of the Science Foundation Ireland (SFI) under investigator award 02/IN.1/172 and the EC-funded Network of Excellence P*h*OREMOST (FP6/2003/IST/2-511616) are gratefully acknowledged. V. L. is grateful to PBCT grant ACT027, Chile, and Rede Nacional de Pesquisa em Nanotubos de Carbono (CNPq), Brazil. The contributions of N. Roos and T. P. Sidiki to the design of the MBE reactor are also acknowledged. We thank A.C. Martín at the Instituto de Microelectrónica de Madrid, CISC, for MBE deposition of Ti/Pt/Au bottom contacts on selected samples and D. Lebedev at the Lehrstuhl für

Mikrostrukturtechnik, FB 13 Elektronik, University of Wuppertal, Germany for ellipsometric characterisation. We also grateful to C. Gergely and P. Arcade of the Groupe d'Etudes des Semiconducteurs, Université Montpellier II, for access to their far-IR spectrometer.

Author contributions

C.O.D, M.S. and C.M.S.T. conceived and designed the experiments and analyses. C.O.D., M.S. and G.V performed the experiments. C.O.D, M.S, G.V., and V.L. analysed the data. S.B.N. conducted part of the TEM analysis and C.M.S.T. supervised the work. All authors discussed the results, and C.O.D. wrote the manuscript.

Additional information

Supplementary Information accompanies this paper at www.nature.com/naturenanotechnology. Reprints and permission information is available online at http://npg.nature.com/reprintsandpermissions/. Correspondence and requests for materials should be addressed to C.O.D.

Competing financial interests

The authors declare no competing financial interests.

Methods

Molecular beam epitaxial deposition and nanowire growth

Prior to ITO growth on silicon and glass substrates, and on Si/SiGe MQW structures, the respective surfaces were cleaned using a standard RCA process where the sample was immersed in a H_2O_2:NH_4OH:H_2O (1:1:1) solution at 80^{o}C for 30 min. After rinsing in deionised water, a second treatment was performed in a H_2O_2:HCl:H_2O (1:1:5) solution with subsequent rinsing in deionised water. Through this process metallic and organic contamination is removed. In the latter step, the surface is oxidized so that a thin (~7 nm) and clean SiO_2 layer forms at the surface. Dipping the sample in HF shortly before introducing it into the evaporator removes the oxide layer and passivates the surface with hydrogen. For evaporation of the In and Sn sources, a home-built MBE high vacuum chamber with two distinct effusion cells for In and Sn together with an electron-beam evaporator, was designed in cooperation with MBE-Komponenten GmbH, Germany, with calibrated growth rates. During nanowire growth the sample surface was annealed at temperatures in the range 300^o-650^{o}C. The In:Sn (90:10) was evaporated at growth rates in the range 0.02-0.2 nm s^{-1} up to maximum temperature for In and Sn of T_{In} = 835^{o}C, T_{Sn} = 1000^{o}C, respectively.

For transparency studies, a glass control substrate was also mounted in the growth chamber in tandem with the Si/SiGe MQW. ITO nanowire layers deposited on glass were used to determine the sheet resistance and the transparency of a similar layer to that grown on the device. The growth parameters were chosen to achieve a transparency of at least 90% in the 1.2-1.6 μm SiGe emission range and sheet resistivities in the range 1-4 × 10^{-4} Ω cm. A substrate growth temperature T_{sub} = 575^{o}C gave a sheet resistivity of 1.7 × 10^{-4} Ω cm when both In and Sn were deposited at a rate of 0.2 nm s^{-1}.

Electron Microscopy

The morphological characterization of the nanowire layers was performed by field emission scanning electron microscopy (FESEM) using a Hitachi S-4800 operating at beam voltages between 5-30 kV. Electron transparent specimens were prepared by ion-milling techniques and placed on a holey carbon support. Transmission electron microscopy (TEM) and selected area electron diffraction (SAED) were conducted using a JEOL JEM-2000FX TEM operating at 200 kV and a Philips CM300 FEGTEM operating at 300 kV. Focused ion beam (FIB) milling was conducted using a FEI 200 FIBSIMS Workstation.

X-ray Diffraction

X-ray diffraction and reflectivity measurements were performed using a high-resolution X-ray diffractometer (Rigaku SLX-2000). A rotating anode Cu Kα source (λ = 0.15418 nm, 18 kW) was used and the X-ray beam was monochromatized using a channel-cut Ge(220) monochromator. The incident and reflected beams were collimated with slits of 0.05 mm in width and the reflection intensity was measured by a scintillation counter.

Electro- and Photoluminescence/Reflectance Measurements

Optical excitation came from a 6 W Argon ion (Ar^+) laser (Spectra Physics *Stabilite* 2017) operating at 514.5 nm. Luminescence was collected through a SPEX 1680 double monochromator into a cooled North Coast EO-817L Ge detector. For photoluminescence (PL) and electroluminescence (EL) measurements, a pulsed excitation optical signal with a fixed frequency of 590 Hz and an electrical signal pulsed at 570 Hz, respectively, were used and modulated by a mechanical chopper. The output from the chopper was fed through a lock-in amplifier measuring the output signal of the Ge detector sensitive in a spectral range 0.8-1.7 μm. Reflectance measurements were carried out in a Bruker FT-IR spectrometer IFS66/V. Different configurations of beamsplitters, detectors and sources were used to cover the spectral range

from a far infrared ($10\ cm^{-1}$) to near infrared and visible ranges. For angular resolved measurements, a NIR512 Ocean Optics spectrometer was used as a detector in a home-built reflectance/transmittance setup.

Comparative photo- and electroluminescence (PL/EL) measurements were performed on Si/SiGe MQW LEDs grown by MBE. To compare the optical transmission, an ITO nanowire layer and a 30 nm NiCr metal contact were deposited on two separate samples on the same substrate. As a reference, the photoluminescence spectrum of an uncoated MQW structure was recorded under identical conditions.

Si/SiGe Multi Quantum Well LED and Electrical Characterization

The n-i-p^+ Si/SiGe multi quantum well (MQW) structures were grown by molecular beam epitaxy (MBE). On an 80 nm undoped Si buffer grown at 700°C on Si(001), a 15-period $Si/Si_{0.77}Ge_{0.23}$ (4.1 nm/3.9 nm) quantum well structure was deposited at 625°C. The entire structure was capped with 42 nm B-doped ($5 \times 10^{18}\ cm^{-3}$) Si to saturate SiGe dangling bonds. After an additional 10 nm Si top layer grown at 625°C, a capping layer of 30 nm p^+-Si (P-doped) was grown at 700°C. The back contact was a Ti (50 nm diffusion barrier)/Pt (50 nm)/Au (100 nm) multilayer ohmic contact. Several structures were top-contacted with a Ni/Cr bilayer deposited by sputtering. Electrical characterization was performed at room temperature in ambient conditions. Resistivity measurements were conducted using a four-point probe system from Jandel Engineering Ltd., and mobility measurements were acquired with a Andeen-Hagerling Model 2550A capacitance bridge and a BioRad Polaron Division Hall Measuring System HL5200. All current-voltage (I-V) measurements were conducted with a HP Semiconductor Parameter Analyzer 4145A.

References

[1] Transparent conducting oxides. *MRS Bull.* (Special issue) **25**, (2000).

[2] Wan, Q. *et al.* High-performance transparent conducting oxide nanowires. *Nano Lett.* **6**, 2909-2915 (2006).

[3] Sawada, M., Higuchi, M., Kondo, S. & Saka, H. Characteristics of indium-tin-oxide/silver/indium -tin-oxide sandwich films and their application to simple-matrix liquid-crystal displays. *Jpn. J. Appl. Phys.* **40**, 3332-3336 (2001).

[4] Kim, H., Horwitz, J. S., Kim, W. H., Kafafi, Z. H. & Chrisey, D. B. Highly oriented indium tin oxide films for high efficiency organic light-emitting diodes. *J. Appl. Phys.* **91**, 5371-5376 (2002).

[5] Synowicki, R. A., Hale, J. S., Ianno, N. J. & Woollam, J. A. Low earth orbit effects on indium tin oxide and polyester and comparison with laboratory simulations. *Surf. Coat. Technol.* **62**, 499-503 (1993).

[6] Granqvist, C. G. & Hultåker, A. Transparent and conducting ITO films: new developments and applications. *Thin Solid Films* **411**, 1-5 (2002).

[7] Kim, D.-W. *et al.*, Highly conductive coaxial SnO_2-In_2O_3 heterostructured nanowires for Li ion battery electrodes. *Nano Lett.* **7**, 3041-3045 (2007).

[8] Cui, Y. & Lieber, C. M. Functional nanoscale electronic devices assembled using silicon nanowire building blocks. *Science* **291**, 851-853 (2006).

[9] Hsu, Y.-J. & Lu, S.-Y. Vapor-solid growth of Sn nanowires: Growth mechanism and superconductivity. *J. Phys. Chem. B* **109**, 4398-4403 (2005).

[10] Zhou, J. *et al.*, Vertically aligned Zn_2SiO_4 nanotube/ZnO nanowire heterojunction arrays. *Small* **3**, 622-626 (2007).

[11] Lu, J. G., Chang, P. & Fan, Z. Quasi-one-dimensional metal oxide materials-Synthesis, properties and applications. *Mater. Sci. Eng. R* **52**, 49-91 (2006).

[12] Johnson, M. C., Aloni, S., McCready, D. E. & Bourret-Courchesne, E. Controlled vapor-liquid-solid growth of indium, gallium, and tin oxide nanowires via chemical vapor transport. *Cryst. Growth Des.* **6**, 1936-1941 (2006).

[13] Nguyen, P. *et al.* Epitaxial directional growth of indium-doped tin oxide nanowire arrays. *Nano Lett.* **3**, 925-928 (2003).

[14] Xiang, J., *et al.* Ge/Si nanowire heterostructures as high-performance field-effect transistors. *Nature* **441**, 489-493 (2006).

[15] Law, M., Greene, L. E., Johnson, J. C., Saykally, R. & Yang, P. D. Nanowire dye-sensitized solar cells. *Nature Mater.* **4**, 455-459 (2005).

[16] Dattoli, E. N. *et al.* Fully transparent thin-film transistor devices based on SnO_2 nanowires. *Nano Lett.* **7**, 2463-2469 (2002).

[17] Wang, D. L. & Lieber, C. M. Inorganic materials: Nanocrystals branch out. *Nature Mater.* **2**, 355-356 (2003).

[18] van der Pauw, L. J. A method of measuring specific resistivity and Hall effect of discs of arbitrary shape. *Philips Res. Repts*. **13**, 1-9 (1958).

[19] Wan, Q., Feng P. & Wang T. H. Vertically aligned tin-doped indium oxide nanowire arrays: Epitaxial growth and electron field emission properties. *Appl. Phys. Lett.* **89**, 123102-4 (2006).

[20] Zhang, L., Tu, R. & Dai, H. J. Parallel core-shell metal-dielectric-semiconductor germanium nanowires for high-current surround-gate field-effect transistors. *Nano Lett.* **6**, 2785-2789 (2006).

[21] Nguyen, P. *et al.* Direct integration of metal oxide nanowire in vertical field-effect transistor. *Nano Lett.* **4**, 651-657 (2004).

[22] Ju, S. *et al.* Fabrication of fully transparent nanowire transistors for transparent and flexible electronics. *Nature Nanotech.* **2**, 378-384 (2007).

[23] Kim, J. K. *et al.* Light extraction enhancement of GaInN light emitting diodes by graded refractive index indium tin oxide anti-reflection contact. *Adv. Mater.* **20**, 801-804 (2008).

[24] Weber, J. & Alonso, I. Near-band-gap photoluminescence of Si-Ge alloys. *Phys. Rev. B* **40**, 5683-5693 (1989).

[25] Schnitzer, I., Yablonovitch E., Caneau, C., Gmitter, T. J. & Scherer, A. 30% external quantum efficiency from surface textured, thin-film light-emitting diodes. *Appl. Phys. Lett.* **63**, 2174-2176 (1993).

Figure captions

Figure 1: **ITO nanowire nucleation and growth.** (a) Plan-view SEM image of oxidized In-Sn droplet seed crystals under MBE deposition conditions of T_{sub} = 400^{o}C, T_{In} = 835^{o}C, T_{Sn} = 1000^{o}C and at a rate of 0.1 nm s^{-1}. These seeds nucleate the precipitative growth of the nanowire. Scale bar = 100 nm. (b) Cross-sectional SEM image of the interior of the nanowire layer grown at T_{sub} = 400^{o}C at nominal In:Sn (90:10) growth rates of 0.1 nm s^{-1}. Scale bar = 50 nm. (c) SEM image of the faceted seed crystal-nanowire interface. (d) The higher magnification HRTEM image and associated SAED pattern clearly identify the monocrystalline cubic $(In_{1.875}Sn_{0.125})O_3$ phase with (002) and (020) interplanar spacings of 0.506 nm. (e) Large area EDX spectrum of the nanowire layer showing the In and Sn L-edge lines, O and Si substrate lines.

Figure 2: **Electrical characterisation of ITO nanowire/SiGe MQW contacts.** (a) Cross-sectional SEM images of the nanowire layer on a SiGe MQW. The nanowire layer shown was grown at a substrate temperature of T_{sub} = 575^{o}C at a growth rate of 0.2 nm s^{-1} and an invariant oxygen partial pressure of 2.1 × 10^{-4} mbar. (b) Schematic representation of the ITO nanowire contacted SiGe MWQ LED. The active region consists of a 15 period Si/$Si_{0.77}Ge_{0.23}$/Si multiple quantum well layer. The bottom contact is a Ti/Pt/Au trilayer. The nanowires were grown directly onto the p^{+}-Si. (c) Room temperature (295 K) I-V characteristics of the Si/SiGe MQW LED acquired in the absence of illumination. (*Inset*) I-V characteristics of the ITO/p^{+}-Si ohmic contact. (d) Free carrier field effect mobility (●) and density (■) of the ITO nanowires as a function of oxygen pressure during growth. The nanowires examined were grown at a rate of 0.2 nm s^{-1} at T_{sub} = 575^{o}C, T_{In} = 835^{o}C, T_{Sn} = 1000^{o}C.

Figure 3: **Optical transmission characteristics of ITO nanowire layers.** (a) Transmission measurements of an ITO nanowire layer deposited at a substrate temperatures of T_{sub} = 575°C (——) and T_{sub} = 450°C (——) at a nominal growth rate of 0.05 nm s^{-1} and an invariant oxygen partial pressure of 2.1 × 10^{-4} mbar. The inset shows an ITO nanowire layer deposited on a glass cover slip. (b) Reflectance spectra for (——) a thin ITO antireflection coating, (——) a porous ITO layer, (——) an ITO nanowire layer (all on silicon) and (·····) a thin ITO film on glass. Plan view SEM images of each layer are also shown. (c) Room temperature (295 K) electroluminescence (EL) spectrum from an ITO nanowire-contacted Si/SiGe MQW structure acquired at an injection current of 575 mA. The $SiGe^{NP}$ (no phonon) and $Si^{TO}_{B\text{-}B}$ (band-to-band transverse optical phonon) emission were extracted with a multiple Gaussian fit.

Figure 4: **Photo- and electroluminescence emission from ITO nanowire-contacted SiGe MQW LED.** Comparison of the low temperature (45 K) photoluminescence spectra of (a) a non-contacted SiGe MQW (——) and a NiCr contacted SiGe MQW (——) (b) a non-contacted SiGe MQW (——) and an ITO nanowire-contacted SiGe MQW (——). The two high intensity peaks observed at 1125 and 1150 nm correspond to the silicon transverse optical phonon-assisted bound exciton recombination (Si_{BE}^{TO}) and the silicon electron-hole droplet emission (Si^{EHD}), respectively. (c) Temperature dependent electroluminescence spectra from the Si/SiGe MQW acquired at a constant driving current of 575 mA in the range 45-295 K. The supplied power causes device heating, thus limiting the lowest temperature to ~45 K inside the cryostat. Luminescence is preserved up to room temperature. (d) The series of SEM images of the nanowire layer highlights the overall long areal range uniformity of growth into dedicated fully transparent contact layers. The scale bar on the first image represents 1 µm. Each successive image (boxed region) was acquired with a magnification increase of ×4. These ITO nanowires have average cross-sectional diameters of 10-15 nm.

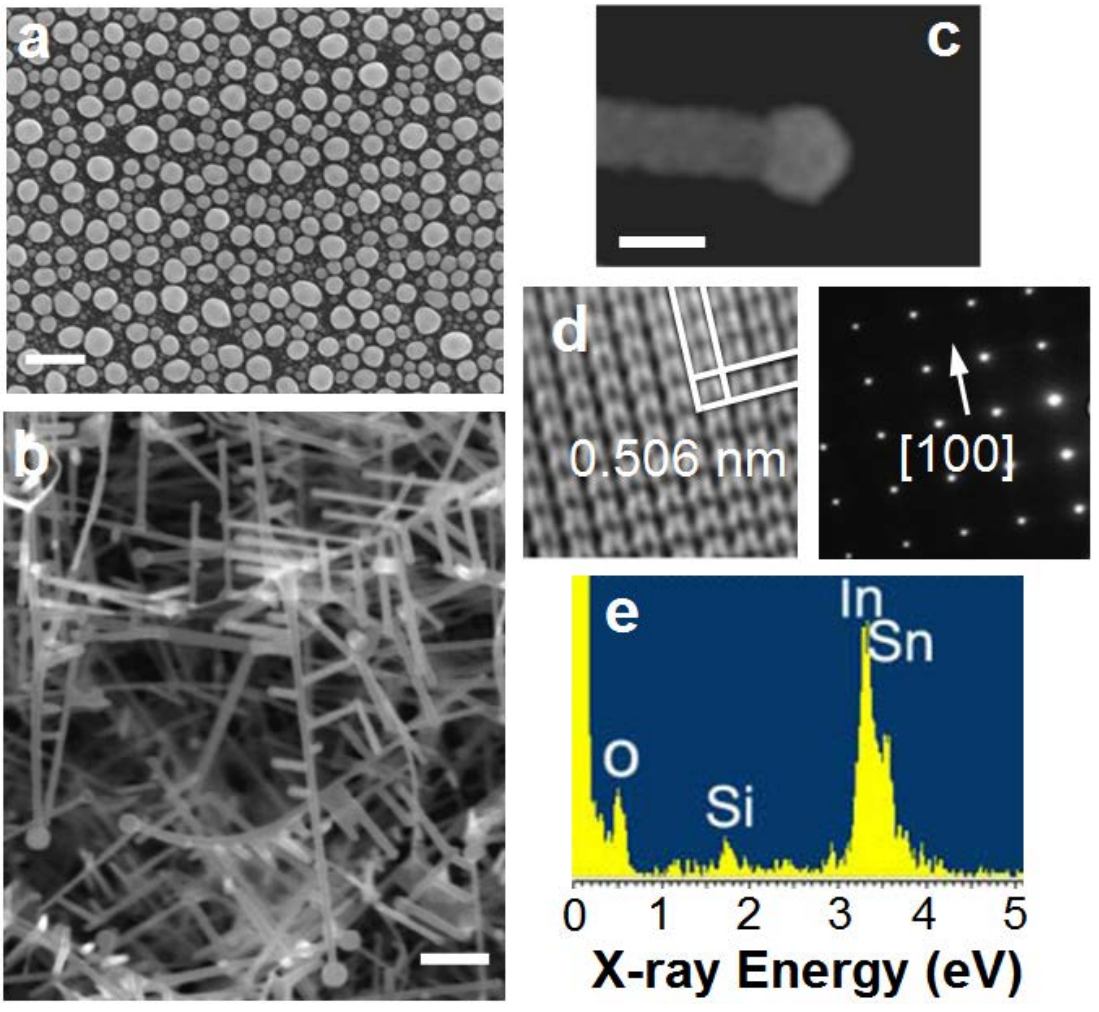

FIGURE 1

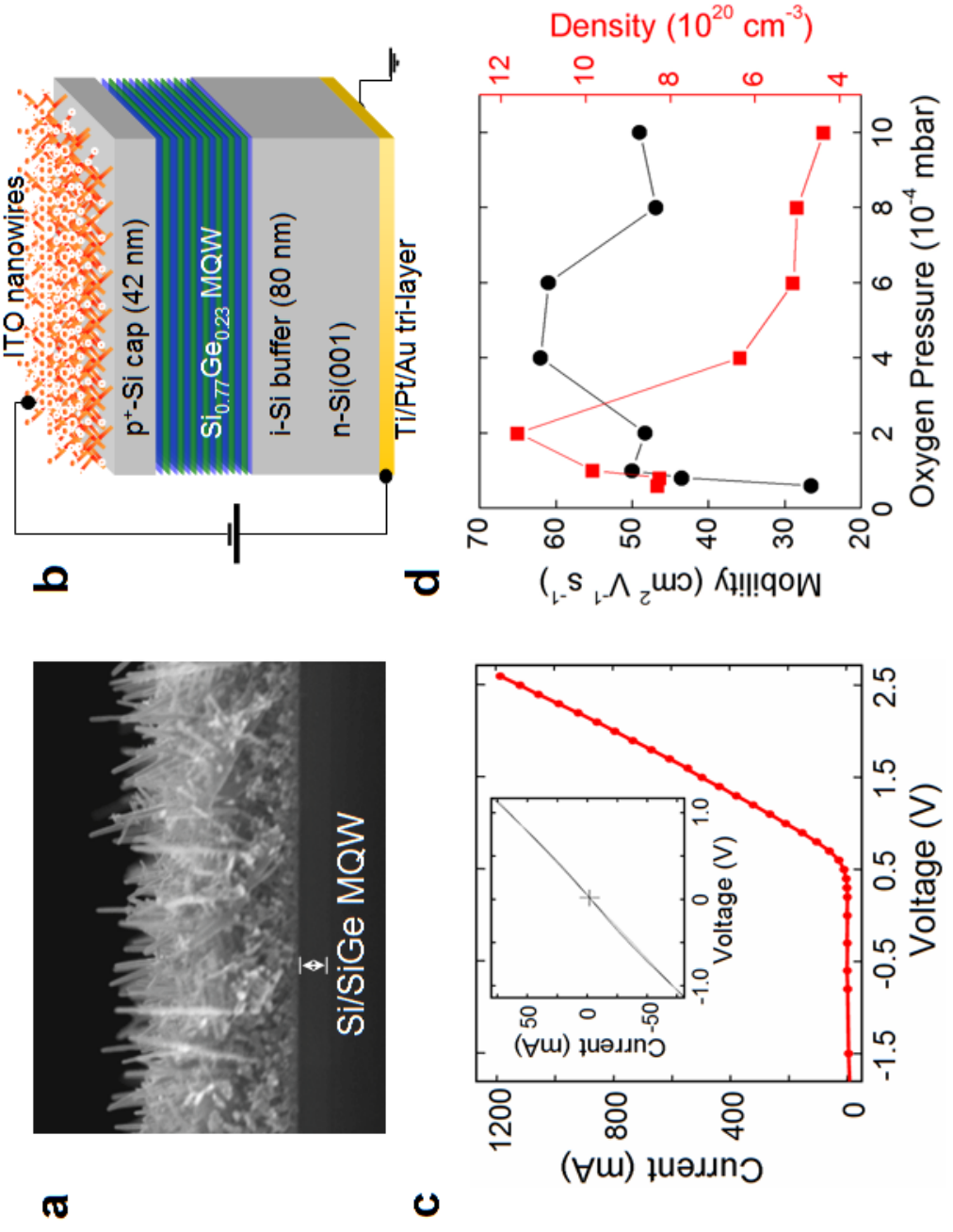
a
Si/SiGe MQW
b
ITO nanowires
p+-Si cap (42 nm)
Si0.77Ge0.23 MQW
i-Si buffer (80 nm)
n-Si(001)
Ti/Pt/Au tri-layer
c
Current (mA)
Voltage (V)
Current (mA)
Voltage (V)
d
Density (10^20 cm^-3)
Mobility (cm^2 V^-1 s^-1)
Oxygen Pressure (10^-4 mbar)

FIGURE 2

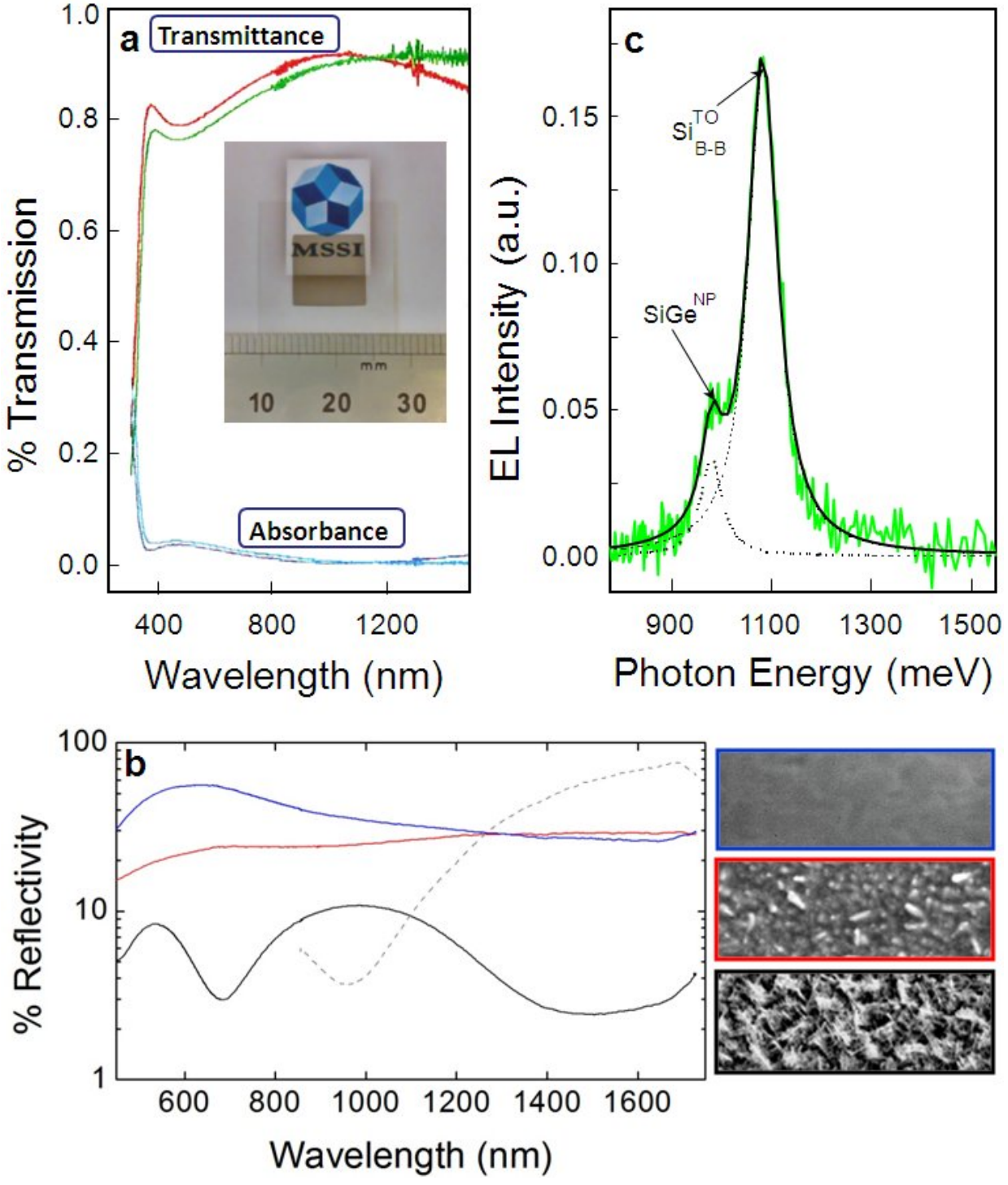
a
Transmittance
Absorbance
% Transmission
Wavelength (nm)
MSSI
mm
10 20 30
c
EL Intensity (a.u.)
Photon Energy (meV)
Si TO B-B
SiGe NP
b
% Reflectivity
Wavelength (nm)

FIGURE 3

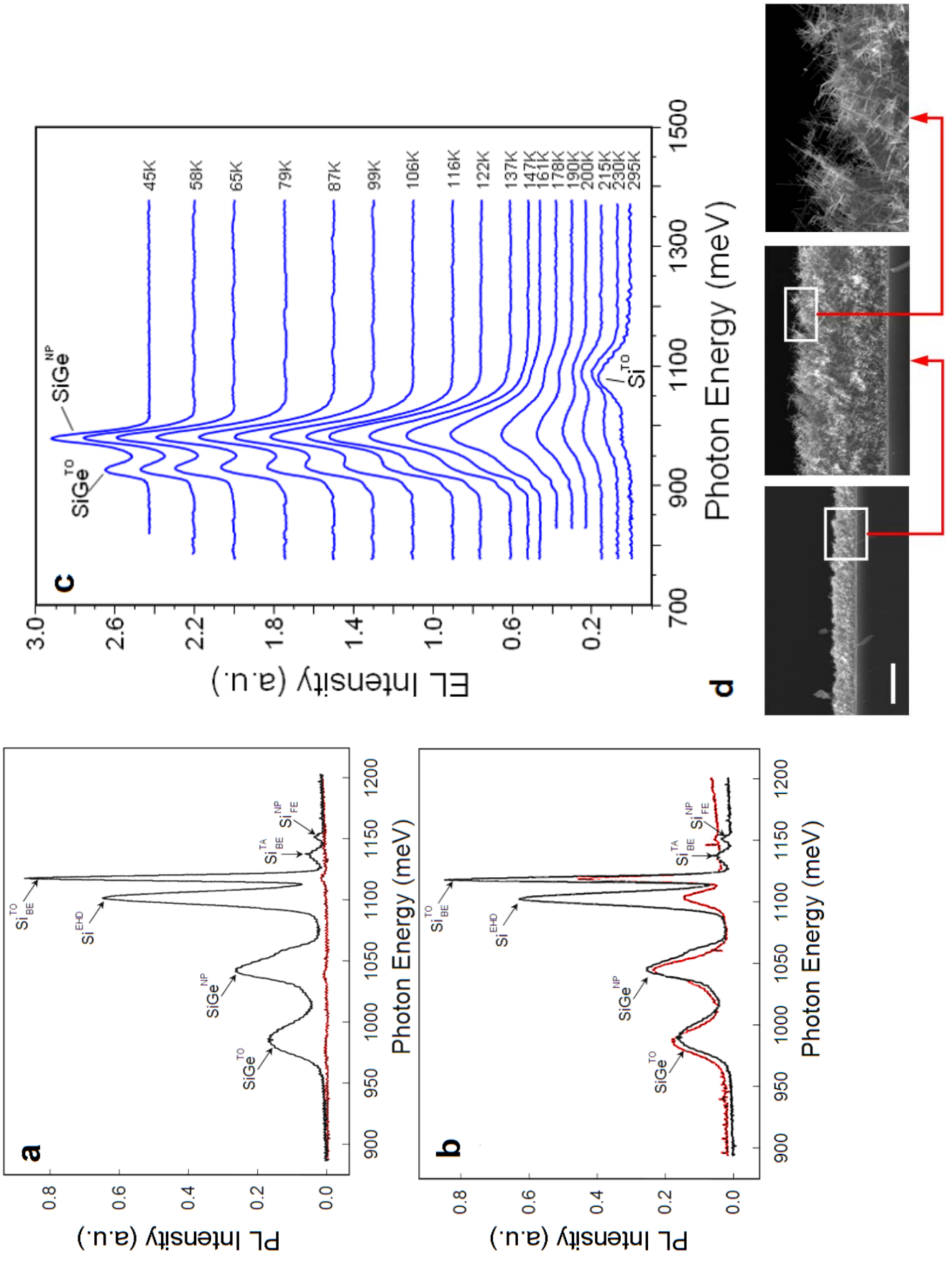
a
b
c
d
PL Intensity (a.u.)
Photon Energy (meV)
EL Intensity (a.u.)
Si_{BE}^{TO}
Si^{EHD}
$SiGe^{NP}$
$SiGe^{TO}$
Si_{BE}^{TA}
Si_{FE}^{NP}
Si^{TO}
45K
58K
65K
79K
87K
99K
106K
116K
122K
137K
147K
161K
178K
190K
200K
215K
230K
295K

FIGURE 4